ISSN 1070-4272, Russian Journal of Applied Chemistry, 2023, Vol. 96, No. 12, pp. 1025–1040. © Pleiades Publishing, Ltd., 2023.
Russian Text © The Author(s), 2023, published in Zhurnal Prikladnoi Khimii, 2023, Vol. 96, No. 12, pp. 942–957.

CATALYSIS

CrO_x–SiO_2 Catalysts in Nonoxidative Propane Dehydrogenation: Effect of Adding Cerium Dioxide

I. Yu. Kaplin[a,*], E. V. Golubina[a], A. V. Gorodnova[a], E. S. Lokteva[a], M. A. Galkin[a], A. V. Fionov[a], O. Ya. Isaikina[a], A. V. Shumyantsev[a,b], and K. I. Maslakov[a]

[a] *Department of Chemistry, Moscow State University, Moscow, 119991 Russia*
[b] *All-Russia Institute of Scientific and Technical Information, Russian Academy of Sciences, Moscow, 125190 Russia*
**e-mail: kaplinigormsu@gmail.com*

Received December 12, 2023; revised December 20, 2023; accepted December 29, 2023

Abstract—The effect that introduction of cerium oxide into oxide systems based on chromium and silicon exerts on the catalytic properties of these systems in nonoxidative propane dehydrogenation in a flow-through system with a fixed catalyst bed was studied. The characteristics of the catalysts CrO_x–SiO_2 and CrO_x–CeO_2–SiO_2, both containing 9 wt % CrO_x assuming the Cr_2O_3 stoichiometry, were compared. The CeO_2 content of the ternary system was 52 wt %. The catalysts were characterized by X-ray diffraction analysis, scanning electron microscopy, Raman spectroscopy, electron paramagnetic resonance, X-ray photoelectron spectroscopy, temperature-programmed reduction with hydrogen, and thermal analysis. In the initial period of the reaction, the catalyst containing CeO_2 demonstrated higher propane conversion at 500 and 550°C and higher deactivation rate compared to CrO_x–SiO_2. Both catalysts can be regenerated by treatment in an air stream at 550°C for 30 min. Cerium dioxide favors the reduction of chromium in high oxidation states to form active reaction sites, Cr^{3+} ions, ensures higher dispersity of the chromium oxides, and favors partial oxidation of coke deposits in the initial period of the catalyst operation.

Keywords: nonoxidative propane dehydrogenation, propylene, oxide catalysts, chromium oxide, cerium oxide, silicon oxide, regeneration

DOI: 10.1134/S1070427223120029

Propylene is a precursor for preparing a wide range of polymer materials. The major fraction of propylene used in the industry is formed as a by-product in cracking of petroleum fractions, but this process is low-selective with respect to propylene and does not meet the steadily growing demand.

The development of commercial technologies for directional synthesis of propylene from propane becomes more and more topical, because the feed for this process is natural gas. Propane can be readily converted to propylene in the course of catalytic oxidative or nonoxidative dehydrogenation. In oxidative dehydrogenation, the addition of an oxidant favors the removal of hydrogen from the reaction mixture, which leads to the shift of the equilibrium and to an increase in the propylene yield. In addition, the oxidizing additive favors the coke burnout from the surface and enhances the catalyst stability. The drawback of this procedure is irreversible loss of the feed in side oxidation reactions. Nonoxidative propane dehydrogenation is free of this drawback, but the optimum thermodynamic yield in this process at a pressure of 1 bar is reached in a narrow temperature interval, 500–600°C. The lower temperature limit is determined by considerable endothermicity of the dehydrogenation reaction ($\Delta_r H°_{298}$ 124.3 kJ mol^{-1}). The upper limit is associated with side processes of the break of C–C bonds, actively occurring at higher temperatures [1, 2] and leading to the formation of large amounts of gaseous by-products. A decrease in the propane partial pressure by decreasing the total pressure and/or propane fraction in the feed [2] leads to an increase in the propane conversion.

Catalytic systems containing chromium oxide [CATOFIN® process (CATOFIN® technology is a process for producing olefins such as propylene (from propane) and isobutylene (from isobutane) using catalysts based on CrO_x/Al_2O_3. Lummus Technology has exclusive license rights for this technology throughout the world [2])] or platinum particles supported on aluminum oxide [C3 OLEFLEX® process (Catalysts of the composition K(Na)–Pt–Sn/Al_2O_3 are used in the C3 OLEFLEX® technology of the Honeywell UOP company for producing propylene from propane [2])] are widely used in commercial processes for nonoxidative dehydrogenation of hydrocarbons. The propane-to-propylene conversion in the presence of these catalysts reaches acceptable values, but the systems in hand are prone to deactivation due to intense coking and require regeneration [2, 3]. The use of platinum catalysts is restricted by high cost of platinum and by the need to redisperse the catalysts sintered in the course of the reaction using chlorine-containing agents, which makes the process environmentally harmful.

Commercial catalysts of the CATOFIN® process have high chromium content. Because of the possible presence of toxic Cr(VI) compounds, these catalysts are potentially hazardous for the health of the personnel of catalytic dehydrogenation facilities and of plants for production of these catalysts. Therefore, the development of alternative platinum-free catalytic systems with low chromium content is an extremely important problem.

Systems based on chromium oxide have complex structure and chemical composition because of variability of the chromium oxidation state in the operating catalyst. Cr^{6+}, Cr^{5+}, Cr^{3+}, and Cr^{2+} compounds can be present in the course of the reaction on the surface of the catalytic system [2, 4]. The Cr^{3+} and Cr^{2+} ions exhibit the catalytic activity, and the particles containing chromium in oxidation states 6+ and 5+ show no catalytic properties in the nonoxidative propane dehydrogenation. The catalytic properties also depend on the dispersity of chromium oxides. Amorphous or finely crystalline Cr_2O_3 particles exhibit high activity, whereas coarse particles of crystalline α-Cr_2O_3 are virtually inactive in the process [5]. In addition, local overheating under reducing reaction conditions can lead to the chemical reaction of chromium oxides with aluminum oxide to form the inactive spinel phase [6]. Increased coking on acid sites of aluminum oxide also leads to a significant decrease in the propane conversion and in the propylene formation selectivity. Thus, the possible way to enhance the performance of chromium-containing catalysts is the use of systems that do not contain aluminum oxide and have low chromium content with the chromium stabilized in the Cr^{3+} state and high dispersity of Cr_2O_3. These goals can be accomplished by using stable supports based on silicon oxide, allowing the uniform and highly dispersed state of the active component to be maintained.

Previously our research team suggested a procedure for preparing catalysts for nonoxidative propane dehydrogenation of the composition CrO_x–ZrO_2–SiO_2 [7]. SiO_2 inactive in this process served as an effective textural stabilizer: It ensured high specific surface area of the catalyst and high dispersity of active component particles. ZrO_2 contains coordination-unsaturated zirconium cations exhibiting intrinsic activity in nonoxidative propane dehydrogenation. In the initial steps of the reaction, these systems at considerably lower chromium content (6 wt %) ensured high rates of propylene formation, well competing with the commercial analog in this respect, but underwent deactivation considerably faster.

CeO_2 is an active component of oxidation catalysts; it is often used as an additive to enhance the stability [8]. Redox reactions readily occur on the CeO_2 surface. Therefore, it can be assumed that this catalyst can also participate in the oxidation of coke deposits on the surface of chromium-containing catalysts and that cerium ions can contribute to redox processes involving the active component. Hence, the addition of cerium oxide can enhance the stability and activity of catalysts for nonoxidative propane dehydrogenation.

This study was aimed at revealing the effect of adding CeO_2 on the catalytic properties of the CrO_x–SiO_2 oxide system in propane dehydrogenation and at elucidating the nature of the effects observed.

EXPERIMENTAL

We used the following chemicals and precursors for preparing the catalysts: $Cr(NO_3)_3 \cdot 9H_2O$ (99.2%, Lenreaktiv, Russia), cetyltrimethylammonium bromide (99%, BioChemica), $Ce(NO_3)_3 \cdot 6H_2O$ (chemically pure grade, REAKhIM, Russia), tetramethylammonium hydroxide (25% aqueous solution, Acros Organics),

and tetraethoxysilane (analytically pure grade, Sigma–Aldrich, catalog no. 78-10-4).

The catalysts were prepared by one-step precipitation of the components using the procedure described in [7]. The dried samples were calcined in air at 600°C for 5 h. The Cr_2O_3–SiO_2 sample is hereinafter designated as CrSi, and the CrO_x–CeO_2–SiO_2 sample, as CrCeSi.

The nominal chromium content of all the samples was 12.7 mol %, or 9 wt % in terms of Cr_2O_3. The CTAB/Cr (for CrSi) or CTAB/(Cr + Ce) (for CrCeSi) molar ratio was 1 : 2 (molar ratio Ce/Si = 1 : 2, mole fraction of Ce 30%, weight fraction in terms of CeO_2 52 wt %). The chromium content of the catalysts was confirmed by atomic absorption spectrometry with a Scientific iCE 3000 device (Thermo Fisher).

The N_2 adsorption–desorption isotherms were recorded with an Autosorb 1 device (Quantachrome). Prior to measurements, the samples were degassed in the device cell for 3 h at 300°C. The specific surface area was calculated by the Brunauer–Emmett–Teller (BET) method. To take into account the contribution of micro- and mesopores correctly, the volume and mean size of the pores were calculated from the adsorption isotherm using the density functional theory. The data treatment and calculations were performed using the program package supplied with the device.

The electron micrographs of the catalysts were taken with a JCM-6000 Neoscope (JEOL) scanning electron microscope (SEM) equipped with an attachment for local energy-dispersive X-ray (EDX) analysis and with a JEM 2100F/UHR (JEOL) transmission electron microscope (TEM).

The Raman spectra were taken with a LabRAM HR 800 UV device (Horiba JobinYvon) using an argon laser with a wavelength of 514 nm. The X-ray photoelectron (XPS) spectra were recorded with an Axis Ultra DLD spectrometer (Kratos Analytical).

The diffraction patterns of the samples were recorded with an Ultima IV powder diffractometer (Rigaku) ($Cu_{K\alpha}$ radiation, 1.5418 Å). The 2θ angle range was 20°–70° with an increment of 0.02°. The phase composition was analyzed using the data from the JCPDS PDF2 library (ICDD database).

Thermal analysis was performed with a STA 449C Jupiter simultaneous thermal analyzer (Netzsch). A weighed portion of a sample was heated from 40 to 900°C at a rate of 10 deg min^{-1} in a gas flow obtained by mixing air (80 mL min^{-1}) and argon (40 mL min^{-1}, grade A, PGS-servis, Russia). In the course of the analysis, we recorded the weight change, thermal effects, and mass spectra of the gas flow at the outlet.

The temperature-programmed reduction with hydrogen (TPR-H_2) was performed with a USGA-101 chemisorption analyzer (UNISIT, Russia). A ~50-mg portion of the catalyst was loaded into a quartz reactor and heated at 150°C for 30 min in an argon flow (grade A, PGS-servis). After that, the reactor was cooled to 30°C and the argon flow was replaced by a flow of the 5% H_2/Ar mixture (technical gas mixture, PGS-servis) fed at a rate of 30 mL min^{-1}. The reactor was linearly heated from 30 to 900°C at a rate of 5, 10, or 15 deg min^{-1}. Changes in the composition of the gas mixture at the reactor outlet were recorded with a thermal conductivity detector. The detector signal was calibrated using the NiO reduction as a reference process. The effective activation energy of the reduction was determined by the Kissinger method using the equation

$$\ln\left(\frac{\beta}{T_m^2}\right) = -\left(\frac{E_A}{R}\right) + \ln\left(\frac{AR}{E_A}\right), \quad (1)$$

where T_m is the temperature corresponding to the maximal reduction rate; β, heating rate; E_A, effective activation energy; A, pre-exponential factor in the Arrhenius equation; and R, universal gas constant.

The electron paramagnetic resonance (EPR) spectra were recorded at room temperature in the X-range (frequency 9.5 GHz) with a Bruker EMX 6/1 radio spectrometer (Bruker) at low microwave radiation power (0.63 mW) when the saturation effect was not manifested. The modulation amplitude was 5 G, and the modulation frequency was 100 kHz.

The nonoxidative dehydrogenation of propane was performed using a fixed-bed tubular quartz reactor with a ULKat-1 flow-through catalytic installation (UNISIT, Russia) equipped with a three-zone tubular furnace, a thermocouple, and temperature and gas flow rate regulators. A 100-mg portion of the catalyst was charged into the reactor between quartz wool beds. The reaction was performed at 500, 550, or 600°C and a total pressure of 1 bar. The catalyst was preliminarily heated to the

reaction temperature in a nitrogen flow (20 mL min^{-1}), after which the reaction mixture (40 vol % C_3H_8, 60 vol % N_2) was fed at a rate F_0 = 30 mL min^{-1} (the catalyst–propane contact time was 8.3 g min L^{-1}). Samples for the analysis were taken at the reactor outlet using a six-way valve switching the gas flow between the gas chromatograph column and chromatographic loop (volume 10 μL).

To characterize coke deposits, 200-mg portions of each catalyst were treated with the reaction mixture at 550°C for 250 min at the same flow rate as in the catalytic experiments, and thermal analysis was performed (thermogravimetric analysis–differential scanning calorimetry, TG–DSC).

The products were analyzed with a Crystal-5000.2 gas chromatograph (Chromatec, Russia) equipped with an HP-PLOT Al_2O_3 S capillary column (length 30 m, 0.53 mm i.d., Agilent) and a flame ionization detector. The retention times and calibration coefficients were preliminarily determined for propane and reaction products by analysis of standard mixtures of known composition (the high-purity gas mixtures were supplied by PGS-servis). The calibration coefficients take into account the sensitivity of the flame ionization detector and the number of carbon atoms in molecules of the starting compound or reaction product.

The propane conversion and product formation selectivity were calculated by Eqs. (2) and (3), respectively.

$$X_{C_3H_8} = \frac{\sum_{i(\text{products})} f(i) A(i)}{\sum_{i(\text{products})} f(i) A(i) + f(C_3H_8) A(C_3H_8)} \times 100, \quad (2)$$

$$S(i) = \frac{f(i) A(i)}{\sum_{i,\,(\text{products})} f(i) A(i)} \times 100, \quad (3)$$

where $A(i)$ and $f(i)$ are the chromatographic peak area and calibration coefficient for ith compound (propylene, methane, ethylene, etc.), respectively.

The initial rate of the propylene formation was estimated using the model of a differential flow-through reactor with a thin fixed catalyst bed:

$$\frac{m_{cat}}{F_{C_3H_8}} = \int_0^{X_{C_3H_8 \to C_3H_6}} \frac{dX_{C_3H_8 \to C_3H_6}}{r_{C_3H_6}} \approx \frac{X_{C_3H_8 \to C_3H_6}}{r_{C_3H_6}}, \quad (4)$$

where $F_{C_3H_8}$ is the molar rate of the propane flow in the reaction mixture (mol min^{-1}), m_{cat} is the weight of the catalyst portion (g), and $X_{C_3H_8 \to C_3H_6}$ is the propane-to-propylene conversion.

The differential character of the reactor was ensured by choosing the reaction conditions so that the propane-to-propylene conversion did not exceed 10%.

Formula (4) can be transformed:

$$r_{C_3H_6} = \frac{F_0 x_{C_3H_6}}{V_m m_{cat}} \approx \frac{\varphi_{C_3H_8} F_0 Y_{C_3H_6}}{V_m m_{cat}}, \quad (5)$$

where F_0 is the total volumetric flow rate (mL min^{-1}); $x_{C_3H_6}$, mole fraction of propylene in the gas mixture at the reactor outlet; $\varphi_{C_3H_8}$, volume fraction of propane in the feed; V_m, molar volume of gases at the temperature of measuring the flow with a gas flow rate regulator; and $Y_{C_3H_6} = (X_{C_3H_8} S_{C_3H_6})$, propylene yield equal to the product of the total propane conversion and selectivity with respect to propylene.

Stability tests were performed with 200-mg portions of the catalyst at 550°C. With the increased catalyst portion, the contact time was 16.6 g min L^{-1}. Approximately 200 min after the start of the reaction, the catalyst was regenerated in the same reactor at 550°C. To this end, the feed supply was stopped, and the catalyst was treated first in an N_2 flow (20 mL min^{-1}, 5 min), then in an air flow (20 mL min^{-1}, 30 min), and finally again in an N_2 flow (5 min). After the regeneration, the feed supply was resumed, and the second cycle of the catalytic experiment was performed.

RESULTS AND DISCUSSION

In our study, we compared CrSi and CrCeSi catalysts containing 9 wt % chromium oxide. At 500°C, the selectivity of both catalysts with respect to propylene appeared to be high and virtually equal (about 90%), but the propane conversion did not exceed 4% (Fig. 1a). In the presence of CrCeSi, the $X_{C_3H_8}$ values appeared to be somewhat higher than with the cerium-free CrSi system and did not decrease with time. This is confirmed by the observed propylene formation rates calculated from the initial propane conversion, selectivity with respect to propylene, and catalyst weight. Thus, in the presence of the CrCeSi system, the initial rate was 0.18, and with the CrSi system, 0.10 mmol min^{-1} g^{-1}.

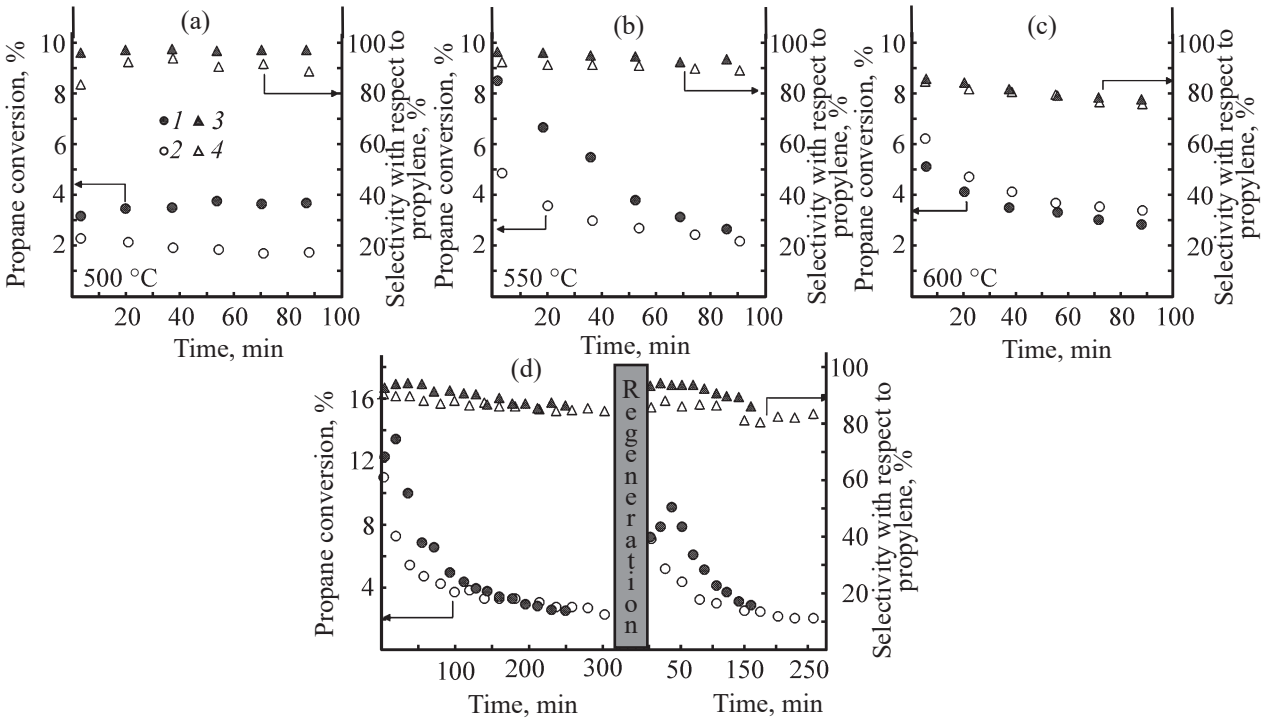

Fig. 1. (*1*, *2*) Propane conversion and (*3*, *4*) selectivity with respect to propylene in nonoxidative propane dehydrogenation in the presence of (*2*, *4*) CrSi and (*1*, *3*) CrCeSi catalysts as functions of time. Isothermal process at (a) 500, (b) 550, and (c) 600°C; (d) operation stability trials at 550°C before and after regeneration by treatment in air for 30 min.

Increasing the reaction temperature to 550°C leads in both catalytic systems to a jumpwise increase in the propane conversion, but with time the conversion drastically decreases because of the coke formation: from 4.9 to 2.2% with CrSi and from 8.5 to 2.7% with CrCeSi (Fig. 1b). In the presence of CrCeSi, the conversion decreases more rapidly. In the presence of CrCeSi, the initial propylene formation rate is approximately 2 times higher than in the presence of CrSi: 0.40 and 0.22 mmol min^{-1} g^{-1}, respectively.

Increasing the temperature to 600°C also leads to a jumpwise increase in the propane conversion in the presence of both samples (Fig. 1c), but at this temperature the propane conversion in the presence of CrSi is higher than in the presence of the CeO_2-containing catalyst. In addition, the selectivity of both systems with respect to propylene appreciably decreases, probably because of the occurrence of side hydrogenolysis reactions. The initial rates of the propylene formation in the presence of CrCeSi and CrSi appeared to be close: 0.23 and 0.27 mmol min^{-1} g^{-1}, respectively.

The catalyst operation stability was checked at 550°C. In this case, the contact time of the feed with the catalyst was longer than in the other experiments. The reaction was performed for 300 min, after which the catalyst was treated for a short time in an air flow to remove coke deposits, and the catalytic trials were resumed (Fig. 1d). In the presence of the cerium-containing sample, we recorded increased propane conversion compared to CeSi in the first 150 min of the reaction both before and after the regeneration. In the curves of the conversion vs. time, there are portions in which the activity of the CrCeSi catalyst changes: The propane conversion first increases and then decreases. In the process, the propylene formation selectivity remains relatively high (80% and higher). Such behavior of the system was not observed when performing trials with a shorter contact time of the catalyst with the feed (Figs. 1a–1c). After the 200-min catalytic runs, the propane conversion decreases to approximately 2–3%. After the regeneration, the activity of both catalysts is partially restored. In the initial time period, the propane

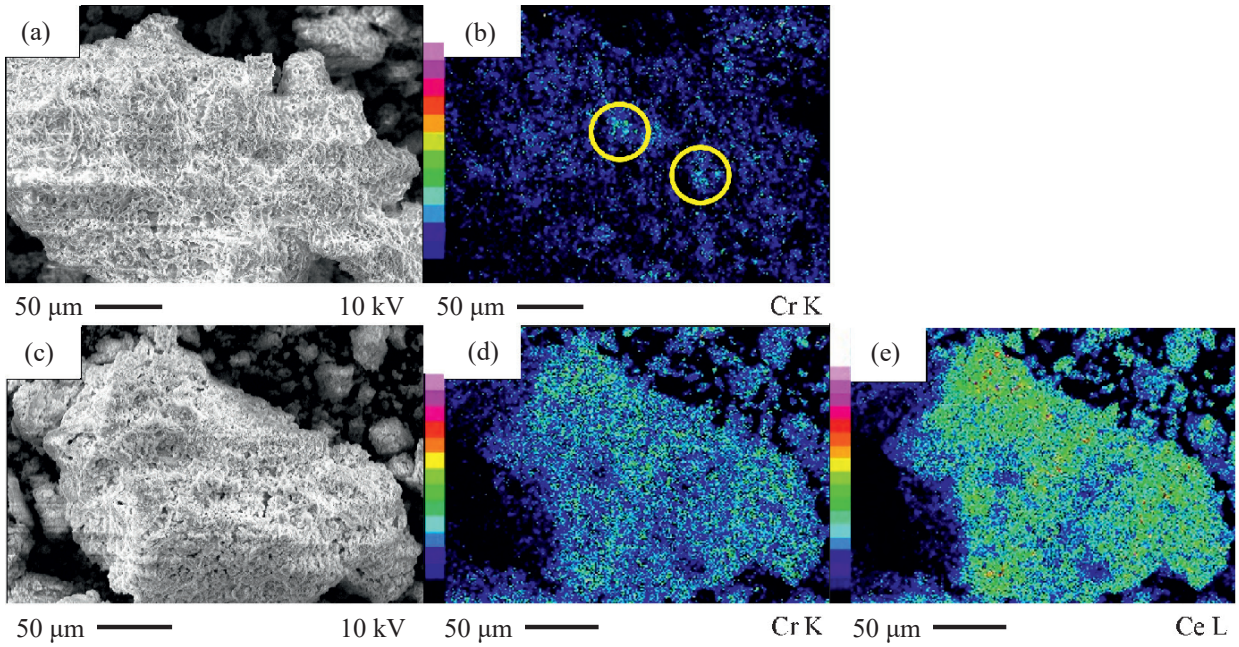

Fig. 2. (a, c) SEM images and EDX distribution maps of (b, d) chromium and (e) cerium on the catalyst surface. Catalysts: (a, b) CrSi (a, b) and (c–e) CrCeSi. Yellow circles show the areas of local chromium concentration on the surface.

conversion on CrCeSi again slightly increases, as in the beginning of the experiment, and then it starts to decrease. The selectivity with respect to propylene after the regeneration remains approximately the same as in the beginning of the trials.

The causes of differences in the catalytic properties were revealed using a set of physicochemical investigation methods. SEM examination (Fig. 2) revealed no significant differences in the morphology of the CrSi and CrCeSi catalysts. Both samples contain agglomerates of particles of various sizes and irregular shape with pronounced spongy porous structure caused by the template synthesis method. According to the SEM–EDX data (Table 1), the Ce : Cr molar ratio is higher than the target ratio (2.65) taken for the synthesis of the CrCeSi system, which can be attributed to heterogeneous distribution of chromium and cerium oxides throughout the sample volume. Such distribution was formed in the course of the solvent removal from the suspensions in the last step of preparing the oxide systems. Regions of chromium localization are seen in the image of the CrSi sample, whereas in the case of CrCeSi the distribution of the elements in the maps is uniform. In addition, in the CrCeSi sample the Cr : Si ratios calculated from the SEM–EDX and XPS data are appreciably higher than in the CrSi sample (Table 1).

Table 1. Physicochemical characteristics of catalysts

Sample	Cr_2O_3,[a] wt %	BET specific surface area, $m^2\ g^{-1}$	Pore volume (DFT), mL g^{-1}	Molar ratio of elements				H_2 uptake at 150–600°C, according to TPR-H_2 data, μmol g^{-1}
				SEM–EDX[b]		XPS[c]		
				Ce : Cr	Cr : Si	Ce : Cr	Cr : Si	
CrSi	8.5	160 ± 20	0.14	–	0.02	–	0.05	670
CrCeSi	8.9	250 ± 30	0.32	7	0.10	3	0.18	1085

Dash indicates that the element is absent in the sample.
[a] Chromium content according to data of atomic absorption spectrometry, calculated assuming the Cr_2O_3 stoichiometry.
[b] Determined by scanning electron microscopy with energy-dispersive X-ray analysis of the chemical composition.
[c] Determined by X-ray photoelectron spectroscopy.

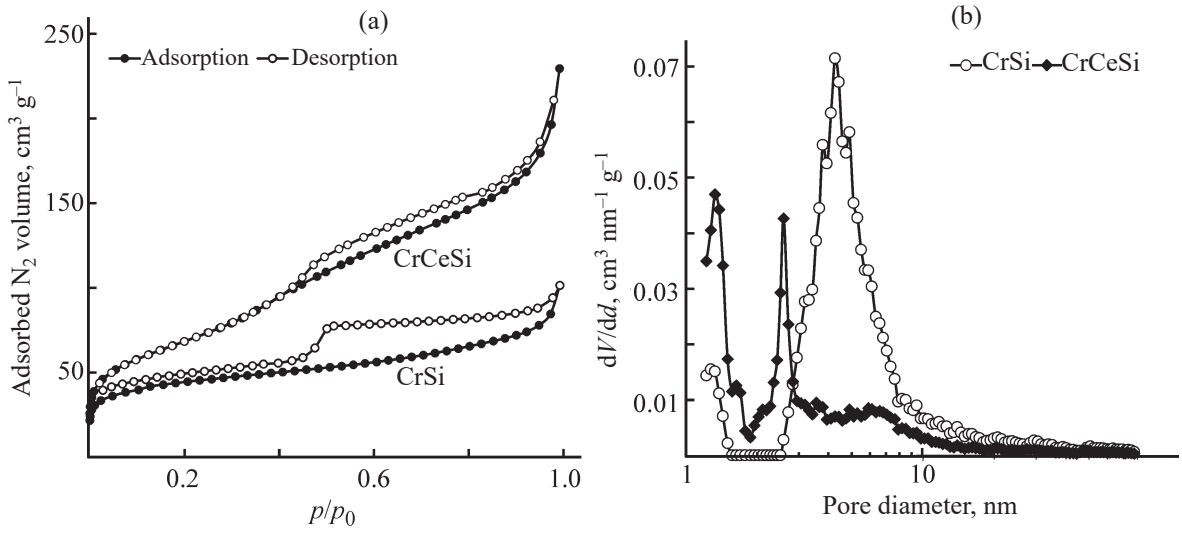

Fig. 3. (a) Isotherms of nitrogen adsorption at 77 K onto CrSi and CrCeSi samples and (b) pore size distribution (DFT method).

Probably, in the presence of cerium, chromium is distributed in the surface and subsurface layers more uniformly, which can positively influence the catalytic activity.

According to the data of low-temperature nitrogen adsorption–desorption, the textural characteristics of the two catalysts differ significantly: The specific surface area and pore volume of the cerium-modified sample, determined by BET and DFT, respectively, are appreciably higher than those of the CrSi sample (Table 1). The causes of this difference become more understandable when considering the results of the adsorption experiments in detail.

The nitrogen adsorption–desorption isotherms (Fig. 3) of the catalysts can be classed with type IV according to IUPAC classification [9]. In both curves, there is a hysteresis loop associated with the effect of the capillary condensation in the mesopores. For the CrSi sample, the hysteresis loop differs in the shape from that characteristic of CrCeSi and has larger size, which is probably caused by higher contribution of mesopores to the structure. At equal relative pressures, the specific volume of nitrogen adsorbed onto CrCeSi is considerably higher compared to the adsorption onto CrSi. Apparently, the CrCeSi sample contains a larger amount of micropores.

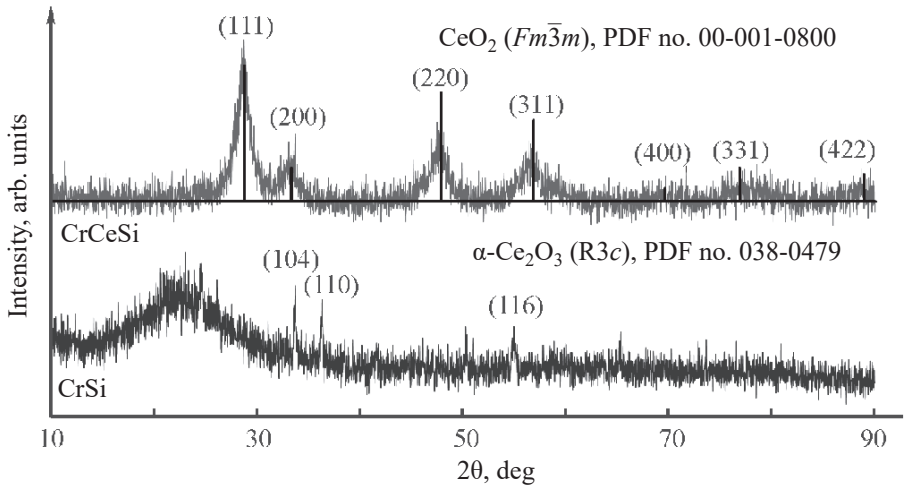

Fig. 4. Powder X-ray diffraction patterns of CrSi and CrCeSi. The reflections of crystalline phases of CeO_2 in CrCeSi and of α-Cr_2O_3 in CrSi are indicated.

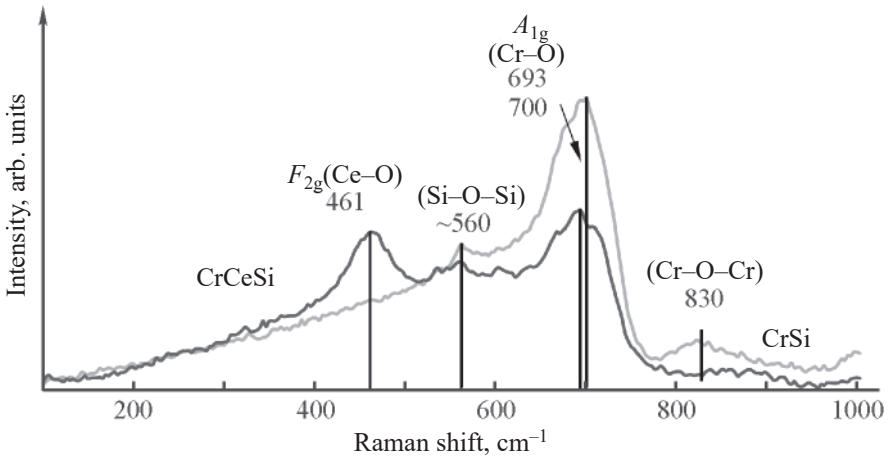

Fig. 5. Raman spectra of CrSi and CrCeSi samples.

This assumption is confirmed by the pore size distribution pattern in the catalysts (Fig. 3b). The distribution was constructed by DFT treatment of the adsorption data. The DFT method allows taking into account the contribution of micropores and fine mesopores to the textural characteristics of the catalysts. The CrSi sample is characterized by the bimodal pore distribution with the prevalent contribution of mesopores and small contribution of micropores. In the pore size distribution of the CrCeSi sample, the contribution of micropores is apparently higher, which accounts for the higher total pore volume and higher specific surface area of this sample. Thus, the adsorption data demonstrate the prevalence of micropores and the finer pore size in the CrCeSi sample compared to the CrSi sample containing predominantly mesopores.

The crystalline structure of the samples is also different. In the X-ray diffraction pattern of the CrSi sample (Fig. 4) at small angles (5°–30°), there are no reflections of crystalline phases of silicon oxides, but there is a halo with a maximum at approximately 22°, caused by the amorphous state of SiO_2 [10]. In addition, in the diffraction pattern there are weak reflections at $2\theta = 33.6°$, 36.2°, 55.1°, corresponding to the crystalline α-Cr_2O_3 phase (space group *R*3*c*, PDF no. 038-1479). The presence of reflections from the crystalline phase indicates that chromium oxide in this catalyst is more coarsely dispersed. Coarser particles of chromium oxide can plug the entrance to micropores and fine mesopores on the SiO_2 surface, which, in combination with larger pore size, accounts for lower S_{BET} and specific pore volume of CrSi.

The diffraction pattern of the CrCeSi catalyst has no pronounced halo, probably because of lower SiO_2 content. On the other hand, the diffraction pattern contains well-defined reflections characteristic of the cubic CeO_2 phase (fluorite crystal type, space group $Fm\bar{3}m$, PDF no. 00-001-0800). However, there are no reflections from crystalline chromium oxides, which suggests their high dispersity in the volume and on the surface of the catalyst. Thus, the dispersity of chromium-containing phases is higher in the CrCeSi sample.

The Raman spectrum (Fig. 5) of the CrSi sample contains two lines: a strong line at 700 cm^{-1} and a weak line at 559 cm^{-1}. The line at approximately 560 cm^{-1} appears in systems containing SiO_2 and is due to vibrations of Si–O–Si bonds [11]. The line at 700 cm^{-1} corresponds to the A_{1g} mode of the Cr–O vibrations in the $[CrO_6]^{9-}$ octahedron [7]. This line is also present in the spectrum of the modified sample, CrCeSi. However, it is somewhat shifted toward lower Raman shifts, which may be due to the interaction between particles of chromium and cerium oxides, and has lower intensity, probably because of higher dispersity of chromium oxides.

In the Raman spectrum of the CrSi sample, there is a weak line near 830 cm^{-1}, which, according to published data [12], appears in the spectra of systems containing dehydrated Cr_2O_3 particles. This mode corresponds to

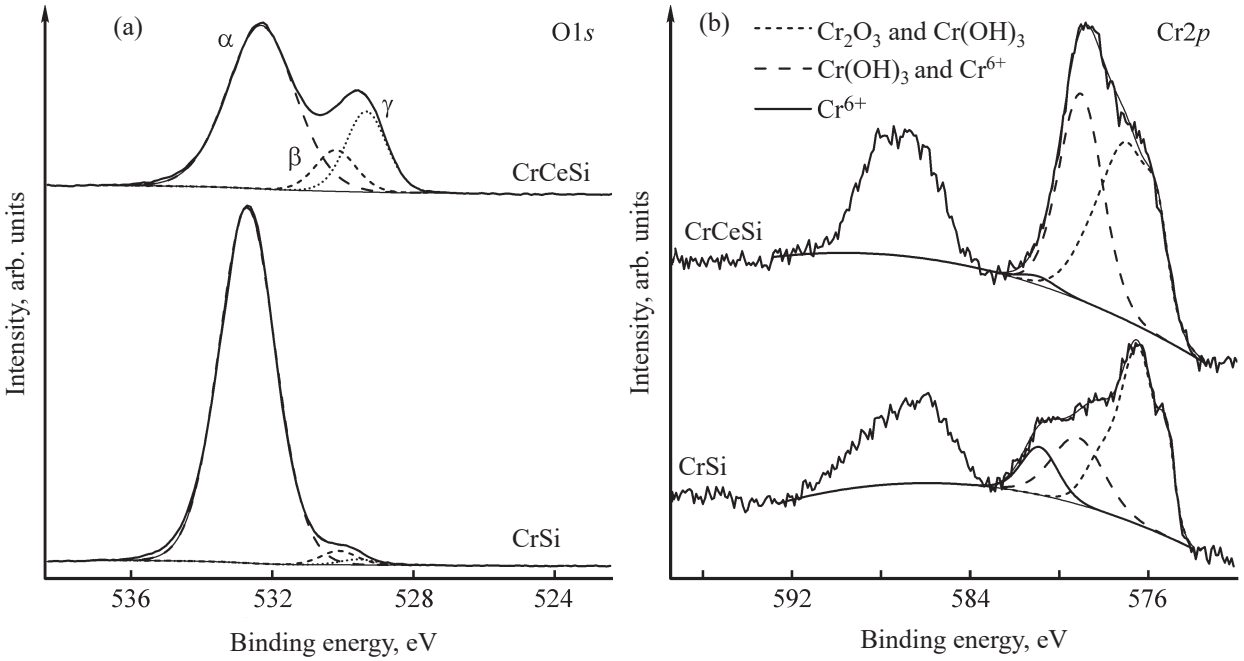

Fig. 6. High-resolution X-ray photoelectron spectra of CrSi and CrCeSi samples: (a) O1*s* and (b) Cr2*p*.

Cr–O–Cr vibrations in polymerized chromates on the surface of chromium oxide [4]. The absence of this signal in the spectrum of CrCeSi can be accounted for by higher chromium dispersity, preventing the formation of coarse Cr_2O_3 particles with high content of polymeric chromates, and by possible interaction between cerium and chromium. In addition, the spectrum of the CrCeSi sample contains a line at 460 cm^{-1}, corresponding to the F_{2g} mode of the Ce–O vibrations in the $[CeO_8]^{12-}$ polyhedron of the cubic CeO_2 lattice [13]. Thus, the Raman data fully agree with the X-ray diffraction (XRD) data.

Specific features of the catalyst surface organization were studied by XPS. In the survey XPS spectra (see Supplementary Materials, Fig. S-1), there are lines of silicon, carbon, oxygen, chromium, and cerium (for CrCeSi). According to the XPS data, the Ce : Cr molar ratio was 3, being close to the value of 2.65 set by the synthesis procedure. This fact indicates that the components on the surface and in deeper subsurface layers of the sample are distributed homogeneously.

To ensure the possibility of qualitative comparison, the spectra of the samples were recorded at equal exposure time. In this case, possible differences between

Table 2. Results of processing high-resolution X-ray photoelectron spectra of O1*s* and Cr2$p_{3/2}$ electrons (CrSi and CrCeSi samples)

Spectrum	CrSi		CrCeSi	
	binding energy, eV	contribution of component in XPS spectrum, %	binding energy, eV	contribution of component in XPS spectrum, %
O1*s*	529.6	1	529.4	20
	530.2	2	530.2	10
	532.7	97	532.4	70
Cr2$p_{3/2}$	576.5	73	577.0	60
	579.2	18	579.1	35
	581.0	9	581.0	5

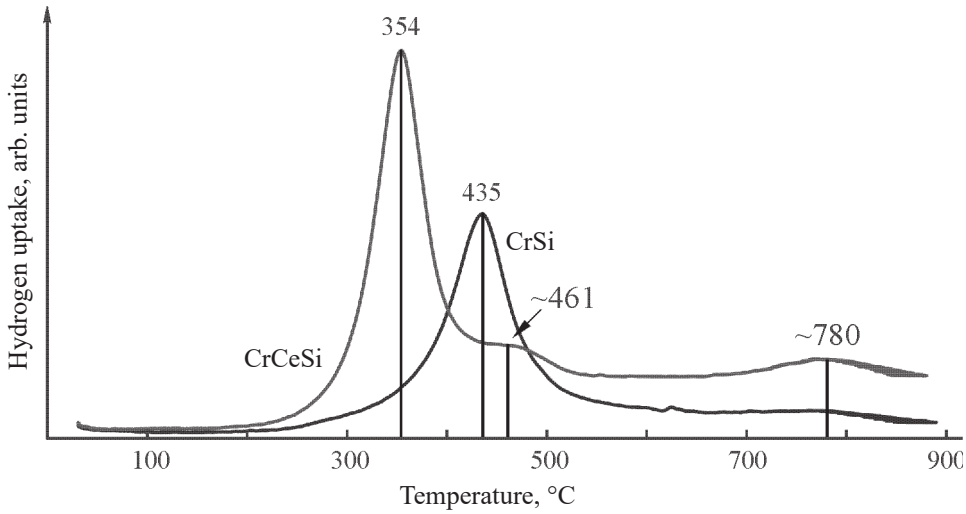

Fig. 7. Profiles of temperature-programmed reduction with hydrogen of CrSi and CrCeSi samples at a heating rate of 10 deg min^{-1}.

the spectra can be reliably interpreted via structural features of the catalysts.

Three components can be distinguished in the XPS spectra of O1*s* electrons (Fig. 6a). The high-energy peak with the maximum at approximately 532.5 eV (α-component, contribution 97 and 70% in the CrSi and CrCeSi systems, respectively; Table 2) is a superposition of the lines with the binding energies of 532 and 533 eV, corresponding to oxygen atoms of Si–O–Si bridges and of surface hydroxyl groups of amorphous SiO_2 [14]. The line at approximately 530.2 eV (β-component) can correspond to oxygen in the structural fragments $Si–O^-$ and Cr–O–H, and the γ-component at 529.5 eV, to the presence of surface oxygen atoms incorporated in the crystal lattices of chromium oxides and CeO_2 and, possibly, in adsorbed oxygen molecules [14–16]. The contribution of this component to the CrCeSi XPS spectrum is considerably higher owing to the presence of the separate CeO_2 phase.

In the XPS spectra of Cr2*p* electrons (Fig. 6b), there is a broad peak in the interval 574–583 eV. Its deconvolution reveals three components. The symmetrical line at approximately 579 eV can be assigned to oxygen-containing Cr(VI) compounds, chromates, and the line at 581 eV, to polychromates and the oxide CrO_3 [17, 18]. The component at 579 eV also contains a contribution from Cr^{3+} in the form of hydroxide fragments [19]. The contributions of these lines in the spectrum of Cr2*p* electrons of CrSi are comparable, whereas in the spectrum of CrCeSi the peak with a maximum at 579 eV is considerably stronger than the second peak, which suggests higher content of highly dispersed chromates and chromium(III) oxide particles on the surface. Thus, the composition of oxides of chromium in high oxidation states is different for the two catalysts, which confirms the conclusions made from the Raman spectra.

The broad asymmetrical line at approximately 577 eV is difficult to interpret. However, the spectra of the two catalysts differ most significantly just for this component: 18 and 35% for CrSi and CrCeSi, respectively. As noted by Biesinger et al. [19], owing to the presence of unpaired valence electrons in Cr^{3+} compounds, the Cr^{3+} signal in the Cr2*p* XPS spectrum undergoes multiplet (so-called exchange) splitting into five components with the maxima in the interval from 575.7 to 578.9 eV, with the contribution from the lowest-energy line being the highest (36%). The same authors note strong broadening of the line with the maximum at 577.3 eV, often assigned to chromium(III) hydroxide. According to their data, the full width at half-maximum of this peak is almost 2.5 eV on the average, which leads to significant overlap with the high-energy Cr^{6+} lines and with Cr^{3+} lines at lower binding energies. The line at 577 eV was also assigned to Cr_2O_3 and to surface Cr^{3+} ions in $Cr(OH)_3$ and CrOOH [20].

Chromium(VI) present on the surface can also be reduced under the conditions of high vacuum in the

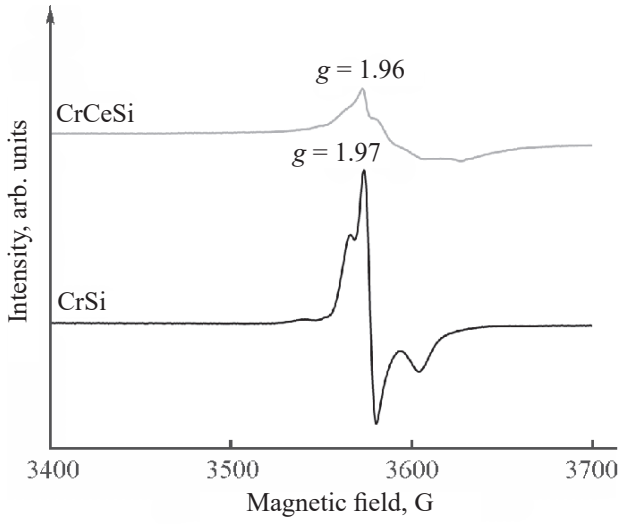

Fig. 8. EPR spectra of CrSi and CrCeSi catalysts. (*g*) Parameter depending on the kind of a paramagnetic particle (Landé factor, or *g*-factor).

course of XPS analysis [21, 22]. In the Ce3*d* XPS spectrum of the CrCeSi sample, the major contribution is from tetravalent cerium ($Ce^{4+}/Ce^{3+} = 31.5$). However, the reduction of cerium oxide is also possible under the conditions of nonoxidative propane dehydrogenation, which have pronounced reducing character. Depending on the specific conditions of the medium and on the catalyst composition, the redox reactions occurring in the process can be shifted toward formation of both more and less oxidized chromium species. For example, in sites of contact of chromium and cerium oxide phases, Cr^{6+} can be reduced to form catalytically active Cr^{3+} sites:

$$3Ce^{3+} + Cr^{6+} = 3Ce^{4+} + Cr^{3+}. \quad \text{(I)}$$

The TPR-H_2 profiles of the two catalysts differ significantly (Fig. 7). In the TPR-H_2 profile of the CrSi sample, there is a strong signal in the region of 350–530°C with the maximum at 435°C, which can be assigned to the reduction of Cr^{6+} dispersed on the SiO_2 surface [23]. The lower total hydrogen uptake in the interval 150–600°C, compared to the TPR-H_2 profile of the modified system (Table 1), suggests the possible presence of crystalline Cr_2O_3, which should be reduced at temperatures higher than 800°C [24]. This is confirmed by the SEM–EDX and XRD data, which reveal in the CrSi sample local accumulations of chromium and crystallites of the Cr_2O_3 phase. SiO_2 is not reduced under these conditions [25].

In the TPR-H_2 profile of the CrCeSi catalyst, the major peak is located at lower temperatures (maximum at 354°C). The shift of the peak toward lower temperatures and a sharp increase in the hydrogen uptake in this region relative to the signal in the TPR-H_2 profile of the CrSi sample suggests an increase in the amount of readily reducible Cr^{6+} sites in the presence of CeO_2. The profile has a weak shoulder with the maximum at 461°C. It is associated with the reduction of highly dispersed Cr_2O_3 particles, which react with hydrogen at a lower temperature compared to the bulk phase [24, 26], and of Ce^{4+} ions on the surface and in CeO_2 near-surface layers [27]. In addition, the profile contains a high-temperature peak at 780°C, indicative of the reduction of the bulk CeO_2 phase [28].

The Kissinger (The Kissinger method is used for treatment of the results of nonisothermal methods (differential thermal analysis, temperature-programmed reduction, etc.) to determine the effective activation energy of chemical processes involving solids.) analysis of the TPR-H_2 profiles recorded at different heating rates allowed us to determine the activation energy of the reduction of chromium in higher oxidation states with hydrogen: 87 ± 3 and 49 ± 4 kJ mol^{-1} for CrSi and CrCeSi, respectively (the linear plots in the Kissinger coordinates are given in Supplementary Materials, Fig. S-2).

The considerable decrease in the activation energy of the Cr^{6+} reduction in the presence of cerium agrees with the previous conclusions that chromium can be reduced via electronic interaction between Ce^{3+} and Cr^{6+} and that the CrCeSi sample contains readily reducible highly dispersed Cr_2O_3 forms, in agreement with the XPS data.

Thus, the presence of cerium under the reaction conditions can favor the chromium transition into active Cr^{3+} forms under the reducing conditions of the propane dehydrogenation and can make these forms more dispersed. This, in turn, should enhance the catalytic activity, especially in the initial period of the reaction, before deactivation of active sites due to coking.

The EPR spectra of the two samples differ significantly (Fig. 8). The spectrum of the CrSi catalyst

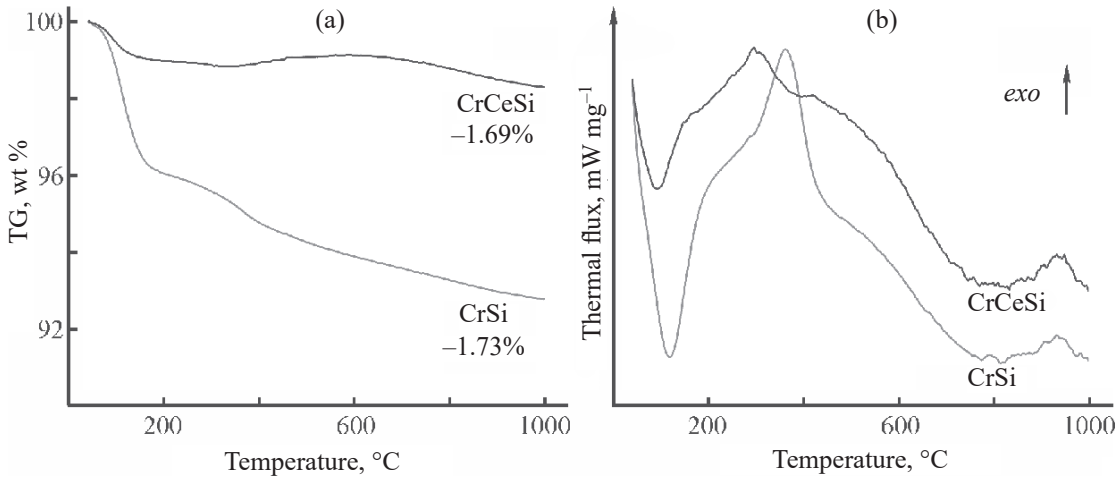

Fig. 9. (a) Thermogravimetric and (b) differential scanning calorimetry curves of the catalysts after the nonoxidative propane dehydrogenation (250 min, 550°C).

contains a composite signal identical to that recorded for the sample of similar composition by Morra et al. [29]. The authors believe that the pseudoaxial signal in the interval g = 1.895–1.979 is due to residual Cr^{5+} ions, which are always present in this system. The signal may also be due to the presence of Cr(VI)–O–Cr(III)–O–Cr(VI) sites in the system. On introducing cerium, the EPR signal becomes broader and sharply decreases in intensity. This is caused by changes in the dispersity and oxidation state of chromium oxide particles in the modified sample. As shown in [30], in CrO_x/CeO_2 chromium is mainly present in the Cr^{3+} state. Probably, a part of chromium atoms occupy the Ce^{4+} sites in the cubic lattice and form Cr–O–Ce bonds, which inhibits further oxidation of Cr. Indeed, in the CrCeSi spectrum, the contribution of the broader anisotropic signal associated with low-spin sites of magnetically isolated Cr^{3+} ions (d^3, S = 1/2) increases. The signal with mean g = 1.96 remains the most pronounced, but its intensity is considerably lower than that in the spectrum of the CrSi system, which is due to the presence of a large amount of highly oxidized chromium forms (chromates, polychromates) and of paramagnetic Ce^{3+} ions in the sample. The presence of such sites and the electronic transitions between them favor the formation of active highly dispersed Cr^{3+} ions under the propane dehydrogenation conditions, which is in agreement with the conclusions made previously from the XPS and TPR-H_2 data.

The thermograms (Fig. 9a) demonstrate the pronounced weight loss caused by the desorption of adsorbed water and burnout of carbon deposits; the weight loss is more pronounced for the CrSi sample. This fact suggests higher coke content of this catalyst. An endothermic process associated with the water desorption occurs up to 200°C (Fig. 9b). At higher temperatures, exothermic carbon burnout starts. For the CrCeSi sample, the exothermic peak has a maximum at 300°C, whereas for the cerium-free system the maximum is shifted toward higher temperatures (about 380°C). This can be attributed to the formation of more readily oxidizable amorphous carbon forms in the CrCeSi sample in the course of catalytic trials. In addition, coke should be removed from the surface of the CrCeSi catalyst in the course of oxidative treatment more readily because of the ability of CeO_2 to donate a certain amount of oxygen from the crystal lattice for the oxidation. This process favors the coke removal even in the course of nonoxidative propane dehydrogenation. As a result, CrCeSi after the catalytic trials contains a smaller amount of coke compared to CrSi, which follows from the thermal analysis data.

The results obtained convincingly explain the differences in the behavior of the catalysts under the conditions of the propane dehydrogenation. Let us consider data obtained in successive runs at different reaction temperatures when the contact time of the feed with the catalyst was 8.3 g min L^{-1}. At 500°C, the initial

propane conversion in the presence of CrCeSi is higher than on CrSi and gradually increases in the course of the reaction, whereas for the unmodified system the propane conversion gradually decreases. The distribution of chromium oxides on the surface of the CrCeSi ternary system is uniform, which is confirmed by higher BET specific surface area and by the absence of local zones of chromium and cerium accumulation according to SEM–EDX data. Apparently, chromium in high oxidation states is partially reduced with Ce^{3+} to form the active highly dispersed Cr_2O_3 phase. This is confirmed by an appreciable low-temperature shift of the signal from the Cr^{6+} reduction in the TPR-H_2 profile of this sample. The coke, which is formed on this catalyst in somewhat smaller amounts, can undergo partial oxidation with the participation of active surface oxygen incorporated in CeO_2. This is indicated by a sharp decrease in the catalyst weight after the catalytic runs in the course of TG–DSC with the heat release at $T < 400$°C. Therefore, coke can be removed even at the lowest reaction temperature used (500°C). It is important that the processes occurring at this temperature, including coking, are slow; therefore, the propane conversion in the presence of the CrCeSi catalyst does not decrease but reaches a steady-state level after the 50-min catalytic run.

At 550°C, the propane conversion on both catalysts in the initial reaction period is appreciably higher than that observed at 500°C, but it strongly decreases in the course of the reaction because of coking. The propane conversion in the presence of CrCeSi is higher compared to CrSi owing to the formation of additional Cr^{3+} sites in redox transformations $3Ce^{3+} + Cr^{6+} = 3Ce^{4+} + Cr^{3+}$ at interfaces of the chromium oxide and CeO_2 phases. This is indirectly confirmed by the Raman, XPS, and EPR data. The absence of the process stabilization step with CrCeSi is associated with the relatively short contact time due to small amount of the catalyst. Under these conditions, the catalyst surface layer is very rapidly reduced, and the rate of the oxygen diffusion from deeper oxide layers is insufficient to ensure efficient oxidation of the soot particles formed. This leads to rapid coking of Cr^{3+} sites, including those formed in the course of catalysis at the interfaces with CeO_2.

At 600°C in the first 50 min, the CrSi sample ensured higher propane conversion compared to the level reached at 550°C. On the contrary, the propane conversion in the presence of CrCeSi was lower than that at 550°C. Increased content of highly dispersed Cr_2O_3 sites in this sample at high reaction temperature favors acceleration of side hydrogenolysis processes leading to coking and degradation of the propane carbon skeleton. In addition, at 600°C in the oxygen-free reaction medium, chromium and cerium oxides can interact with the formation of mixed oxide phases, e.g., perovskites $CeCrO_3$ [31], which increase the oxygen capacity of the system but probably remain stable under the conditions of nonoxidative propane dehydrogenation and do not participate in the reaction redox cycle.

Prolonged runs were performed at longer contact time of the feed with the catalyst (16.6 g min L^{-1}). Under these conditions, the curve of the propane conversion vs. reaction time in the presence of CrCeSi passes through a maximum in the initial period. Probably, with increased amount of active sites contacting with the reaction mixture when taking a larger portion of the catalyst, it becomes possible to detect in more detail the processes occurring on the catalyst surface in the initial reaction period. The increase in the conversion is particularly noticeable when reusing the catalyst after the regeneration. The propane conversion increases in the first 50 min of the reaction and then starts to decrease. The propane conversion immediately after the regeneration is appreciably lower than in the first cycle of the catalyst use. Hence, in the course of short (30 min) regeneration in an air flow, the carbon deposits formed are removed incompletely. Probably, an increase in the propane conversion in the initial period of the second cycle of using the catalyst is caused by additional oxidation of the remaining carbon deposits with oxygen from the crystal lattice of cerium oxide, which diffuses from the bulk of the oxide to the surface where the carbon deposits are located. However, the process is accompanied by partial reduction of the surface and near-surface layers of the catalyst and is accompanied by the appearance of coordination-unsaturated Ce^{3+} ions, as indicated by the XPS and EPR data. These ions are formed by reduction of the surface under the reaction conditions and have no time to undergo oxidation via diffusion of oxygen from the bulk of the CeO_2 cubic lattice. After the surface reduction, the catalyst is deactivated owing to rapid coking on Cr^{3+} sites and partial sintering of chromium oxide phases into coarser crystalline Cr_2O_3 particles, and after a certain period the propane conversion decreases to the level characteristic of the CrSi catalyst. It can

also be assumed that, in the initial period, the residual carbon deposits transform into methane owing to active hydrogen evolution. Indeed, in the initial period of the reaction, both before and after regeneration, methane evolution is observed on CrCeSi. The selectivity with respect to methane is about 2% at this moment, and then the selectivity with respect to methane drastically decreases. However, the CeO_2-free sample exhibits the same behavior. Therefore, the latter assumption cannot account for the evolution of the CrCeSi catalyst in the initial period of the operation.

The results of this study show that introduction of cerium significantly influences the catalytic properties of Cr_2O_3–SiO_2. This influence is primarily determined by the reaction of cerium and chromium ions on the sites of contact, by an increase in the active component dispersity, and by the fact that the carbon deposits formed in the course of nonoxidative propane dehydrogenation on the catalyst can be oxidized with active oxygen from the surface CeO_2 layers. In the future, more detailed study of such systems will allow finding the ways for more efficient CeO_2 dispersion and the optimum conditions for the regeneration of propane dehydrogenation catalysts. Hence, the results obtained open prospects for the commercial use of Cr_2O_3–CeO_2–SiO_2 catalysts.

CONCLUSIONS

The CrSi and CrCeSi catalytic systems are active in nonoxidative propane dehydrogenation. In the initial reaction period, the cerium-containing catalyst ensured higher propane conversion at 500 and 550°C, but underwent deactivation more rapidly. Both samples could be regenerated by short (30 min) treatment in an air flow at 550°C. The presence of cerium oxide in the catalyst can favor higher dispersity of chromium oxides, reduction of chromium in higher oxidation states to form Cr^{3+} ions active in propane dehydrogenation, and partial soot oxidation present in the form of amorphous carbon deposits under the reaction conditions in the initial period of the catalyst operation.

AUTHOR CONTRIBUTION

I.Yu. Kaplin: synthesis of the samples, study of the catalytic activity and stability, interpretation of the results; E.V. Golubina: concept of the study, analysis by scanning electron microscopy and TPR-H_2, interpretation of the results; A.V. Gorodnova: synthesis of the samples, study of the catalytic activity; E.S. Lokteva: formulation of the research direction, interpretation of the results of X-ray diffraction analysis, scanning electron microscopy, and thermal analysis; M.A. Galkin: synthesis of the catalysts, TPR-H_2 experiments; A.V. Fionov: EPR studies and interpretation of the results; O.Ya. Isaikina: Raman studies; A.V. Shumyantsev: TG–DSC studies; K.I. Maslakov: XPS studies and interpretation of the results.

ADDITIONAL INFORMATION

Golubina Elena Vladimirovna, ORCID: https://orcid.org/0000-0002-1040-1428

Kaplin Igor' Yur'evich, ORCID: https://orcid.org/0000-0002-5091-6290

Gorodnova Anastasiya Vsevolodovna, ORCID: https://orcid.org/0000-0001-5116-6770

Lokteva Ekaterina Sergeevna, ORCID: https://orcid.org/0000-0003-3510-4822

Galkin Maksim Aleksandrovich, ORCID: https://orcid.org/0009-0006-5217-854X

Fionov Aleksandr Viktorovich, ORCID: https://orcid.org/0000-0002-6285-9449

Isaikina Oksana Yakovlevna, ORCID: https://orcid.org/0000-0002-4165-6562

Shumyantsev Aleksei Viktorovich, ORCID: https://orcid.org/0000-0002-0166-4912

Maslakov Konstantin Igorevich, ORCID: https://orcid.org/0000-0002-0672-2683

SUPPLEMENTARY INFORMATION

The online version contains supplementary material available at https://doi.org/10.1134/S1070427223120029.

ACKNOWLEDGMENTS

The XPS study was performed using the equipment purchased at the expense of the Moscow University Development Program.

FUNDING

The study was financially supported by the Russian Science Foundation (project no. 22-23-00445).

CONFLICT OF INTEREST

The authors declare that they have no conflicts of interest.

REFERENCES

1. Chen, S., Chang, X., Sun, G., Zhang, T., Xu, Y., Wang, Y., Pei, C., and Gong, J., *Chem. Soc. Rev.,* 2021, vol. 50, no. 5, pp. 3315–3354. https://doi.org/10.1039/D0CS00814A
2. Otroshchenko, T., Jiang, G., Kondratenko, V.A., Rodemerck, U., and Kondratenko, E.V., *Chem. Soc. Rev.,* 2021, vol. 50, no. 1, pp. 473–527. https://doi.org/10.1039/D0CS01140A
3. Huš, M., Kopač, D., and Likozar, B., *J. Catal.,* 2020, vol. 386, pp. 126–138. https://doi.org/10.1016/j.jcat.2020.03.037
4. Weckhuysen, B.M., Wachs, I.E., and Schoonheydt, R.A., *Chem. Rev.,* 1996, vol. 96, no. 8, pp. 3327–3350. https://doi.org/10.1021/cr940044o
5. Michorczyk, P., Pietrzyk, P., and Ogonowski, J., *Micropor. Mesopor. Mater.,* 2012, vol. 161, pp. 56–66. https://doi.org/10.1016/j.micromeso.2012.05.011
6. Shtyka, O., Maniukiewicz, W., Ciesielski, R., Kedziora, A., Shatsila, V., Sierański, T., and Maniecki, T., *Materials,* 2021, vol. 14, no. 12, ID 3218. https://doi.org/10.3390/ma14123218
7. Golubina, E.V., Kaplin, I.Y., Gorodnova, A.V., Lokteva, E.S., Isaikina, O.Y., and Maslakov, K.I., *Molecules,* 2022, vol. 27, no. 18, ID 6095. https://doi.org/10.3390/molecules27186095
8. Li, B., Yuan, X., Li, B., and Wang, X., *Fuel,* 2021, vol. 301, ID 121027. https://doi.org/10.1016/j.fuel.2021.121027
9. Thommes, M., Kaneko, K., Neimark, A.V., Olivier, J.P., Rodriguez-Reinoso, F., Rouquerol, J., and Sing, K.S., *Pure Appl. Chem.,* 2015, vol. 87, nos. 9–10, pp. 1051–1069. https://doi.org/10.1515/pac-2014-1117
10. Tiozzo, C., Bisio, C., Carniato, F., Gallo, A., Scott, S.L., Psaroa, R., and Guidotti, M., *Phys. Chem. Chem. Phys.,* 2013, vol. 15, no. 32, pp. 13354–13362. https://doi.org/10.1039/C3CP51570B
11. Cattaruzza, E., Mardegan, M., Trave, E., Battaglin, G., Calvelli, P., Enrichi, F., and Gonella, F., *J. Non-Cryst. Solids,* 2011, vol. 357, nos. 8–9, pp. 1846–1850. https://doi.org/10.1016/j.jnoncrysol.2010.12.050
12. Khan, T.M. and Irfan, M., *Appl. Phys. A: Mater. Sci. Process.,* 2014, vol. 117, no. 3, pp. 1275–1282. https://doi.org/10.1007/s00339-014-8518-9
13. Loridant, S., *Catal. Today,* 2021, vol. 373, pp. 98–111. https://doi.org/10.1016/j.cattod.2020.03.044
14. Simonsen, M.E., Sønderby, C., Li, Z., and Søgaard, E.G., *J. Mater. Sci.,* 2009, vol. 44, no. 8, pp. 2079–2088. https://doi.org/10.1007/s10853-009-3270-9
15. Al-Kuhaili, M.F. and Durrani, S.M.A., *Opt. Mater.,* 2007, vol. 29, no. 6, pp. 709–713. https://doi.org/10.1016/j.optmat.2005.11.020
16. Scholes, F.H., Hughes, A.E., Hardin, S.G., Lynch, P., and Miller, P.R., *Chem. Mater.,* 2007, vol. 19, no. 9, pp. 2321–2328. https://doi.org/10.1021/cm063024z
17. Liu, B., Fang, Y., and Terano, M., *J. Mol. Catal. A: Chemical,* 2004, vol. 219, no. 1, pp. 165–173. https://doi.org/10.1016/j.molcata.2004.05.001
18. Halada, G.P. and Clayton, C.R., *J. Electrochem. Soc.,* 1991, vol. 138, no. 10, pp. 2921–2927. https://doi.org/10.1149/1.2085340
19. Biesinger, M.C., Payne, B.P., Grosvenor, A.P., Lau, L.W., Gerson, A.R., and Smart, R.S.C., *Appl. Surf. Sci.,* 2011, vol. 257, no. 7, pp. 2717–2730. https://doi.org/10.1016/j.apsusc.2010.10.051
20. Massoud, T., Maurice, V., Klein, L.H., and Marcus, P., *J. Electrochem. Soc.,* 2013, vol. 160, no. 6, pp. C232–C238. https://doi.org/10.1149/2.067306jes
21. Steinberger, R., Duchoslav, J., Greunz, T., Arndt, M., and Stifter, D., *Corros. Sci.,* 2015, vol. 90, pp. 562–571. https://doi.org/10.1016/j.corsci.2014.10.049
22. Golubina, E.V., Kaplin, I.Y., Gorodnova, A.V., Lokteva, E.S., Isaikina, O.Ya., and Maslakov, K.I., *Russ. J. Appl. Chem.,* 2022, vol. 95, pp. 1677–1692. https://doi.org/10.1134/S1070427222110027
23. Hakuli, A., Harlin, M.E., Backman, L.B., and Krause, A.O.I., *J. Catal.,* 1999, vol. 184, no. 2, pp. 349–356. https://doi.org/10.1006/jcat.1999.2468
24. Wang, F., Fan, J.L., Zhao, Y., Zhang, W.X., Liang, Y., Lu, J.Q., and Wang, Y.J., *J. Fluorine Chem.,* 2014, vol. 166, pp. 78–83. https://doi.org/10.1016/j.jfluchem.2014.07.030
25. Kot, M., Wojcieszak, R., Janiszewska, E., Pietrowski, M., and Zieliński, M., *Materials,* 2021, vol. 14, no. 4, ID 968. https://doi.org/10.3390/ma14040968
26. Zhong, L., Yu, Y., Cai, W., Geng, X., and Zhong, Q., *Phys. Chem. Chem. Phys.,* 2015, vol. 17, no. 22, pp. 15036–15045.

https://doi.org/10.1039/C5CP00896D

27. Ranga Rao, G., *Bull. Mater. Sci.,* 1999, vol. 22, no. 2, pp. 89–94. https://doi.org/10.1007/BF02745559
28. Yao, H.C. and Yao, Y.F.Y., *J. Catal.,* 1984, vol. 86, no. 2, pp. 254–265. https://doi.org/10.1016/0021-9517(84)90371-3
29. Morra, E., Martino, G.A., Piovano, A., Barzan, C., Groppo, E., and Chiesa, M., *J. Phys. Chem. C,* 2018, vol. 122, no. 37, pp. 21531–21536. https://doi.org/10.1021/acs.jpcc.8b07699
30. Yang, Q., Surin, I., Geiger, J., Eliasson, H., Agrachev, M., Kondratenko, V.A., Zanina, A., Krumeich, F., Jeschke, G., Erni, R., Kondratenko, E.V., López, N., and Pérez-Ramírez, J., *ACS Catal.,* 2023, vol. 13, no. 24, pp. 15977–15990. https://doi.org/10.1021/acscatal.3c04463
31. Mostrou, S., Büchel, R., Pratsinis, S.E., and van Bokhoven, J.A., *Appl. Catal. A: General,* 2017, vol. 537, pp. 40–49. https://doi.org/10.1016/j.apcata.2017.03.001